JOURNAL OF PROPULSION AND POWER
Vol. 17, No. 4, July–August 2001

Experimental Study of Major Species and Temperature Profiles of Liquid Oxygen/Gaseous Hydrogen Rocket Combustion

Serdar Yeralan,* Sibtosh Pal,† and Robert J. Santoro‡
Pennsylvania State University, University Park, Pennsylvania 16802-2320

Understanding the fundamentals of high-pressure, high-temperature combustion of practical rocket propellants is key to improving rocket engine performance and efficiency. The application of Raman spectroscopy for making detailed species concentration measurements of oxygen, hydrogen, and water vapor in the elevated-pressure, combusting flowfield downstream of a liquid-oxygen/gaseous-hydrogen swirl-coaxial injector element at fuel-rich conditions is presented. Details regarding measurement error analysis and recommendations for further refinement of the diagnostic technique are also presented. To the authors' knowledge, these experiments represent the first time that instantaneous temperature and major species profiles have been successfully made in such an environment. These results, which include both instantaneous and time-averaged temperature and species concentration profiles, impact both rocket fuel preburner design and computational fluid dynamic code validation activities.

Nomenclature

$f(T)$	=	temperature dependent function that relates the spectral bandwidth strength to the signal strength
f	=	focal length
$f/\#$	=	focal length divided by the diameter of the lens
K	=	constant that accounts for the laser pulse energy, species Raman cross section, optical collection efficiency, and optical solid angle
N	=	measurement uncertainty
n	=	number density
S	=	Raman signal intensity
σ_B	=	background shot noise due to flame luminosity
σ_D	=	dark current noise of the intensifier
σ_R	=	Readout noise
σ_S	=	signal shot noise due to Raman signal

Introduction

THE key element of any rocket engine is the injector because it defines the resulting combusting characteristics in terms of mixing, combustion, performance, heat transfer, and stability. Consequently, benchmark quality experimental investigations of injector flowfield development at realistic conditions are important in any engine development program. Results from such experiments can be used for directly assessing the injector design procedure as well as for validating computational fluid dynamics (CFD) models. It is redundant to state that the use of mature experimentally validated CFD codes as a design tool could significantly reduce the cost of engine development programs by reducing the matrix of expensive full-scale testing.

Experimental programs that systematically investigate liquid-oxygen (LOX)/gaseous-hydrogen (GH_2) propellant combustion for rocket injectors at realistic conditions are of paramount importance because of the global usage of this propellant combination for rocket propulsion. In the United States, the LOX/GH_2 propellant combination is currently in use for powering the space shuttle main engines (SSME) and will also be used for the X-33 reusable launch vehicle (RLV). In addition, this propellant combination is being considered for use in future technologies such as the rocket-based combined-cycle and full-flow stage-combustion engine cycle concepts.

A key challenge in providing a better understanding of rocket injectors lies in obtaining suitable measurements in the harsh combustion environment typical of rocket engines. Fortunately, laser-based diagnostic techniques have evolved significantly over the last decade and are continually being refined for application in harsh flowfield environments. For temperature and species measurements in combustion environments, laser-based diagnostic techniques have been successfully used.[1] Although these diagnostic tools, such as Raman spectroscopy and coherent anti-Stokes Raman spectroscopy (CARS), have not been extensively used for characterizing rocket flowfields, they are well-established techniques in studying flames in atmospheric to moderately high (2–8 atm) pressures.[2–8] In recent years, there has been some involvement of laser diagnostics in screening and development of rocket engine injectors. Use of Raman spectroscopy is well incorporated in these investigations, where the technique is suitable.[9–12] Despite the complexity of the experimental systems, CARS has been utilized for rocket plume temperature characterization[13] and laser-induced fluorescence for OH radical measurements in the near-injector region.[14]

The number of studies of LOX/GH_2 combustion has been relatively small due to the extreme nature of the flowfield. The limited number of studies include phase Doppler interferometry measurements of LOX drop size and velocity[15] and flow-visualization studies of injector flowfields at chamber pressures ranging from sub- to supercritical.[16–20]

In this paper, the application of Raman spectroscopy as a diagnostic tool for characterizing the fuel-rich LOX/GH_2 combustion flowfield downstream of a swirl-coaxial injector element is presented. Fuel-rich conditions were chosen because the research impacts immediate and future technology development goals. The gas generator of the proposed YRS2200 engine, which is one option for the X-33 RLV, operates at fuel-rich conditions for LOX/GH_2 propellants. In addition, the preburner for the SSME as well as one of the preburners of the conceptual full-flow staged combustion engine cycle operate under these conditions. The swirl-coaxial injector element was chosen in favor of the shear-coaxial injector element in the present study because earlier efforts indicated that mixing and combustion zone lengths are significantly reduced for the swirl element.[15,18,19]

Experimental Facility

The LOX/GH2 swirl-coaxial flowfield characterization experiments were conducted at the Cryogenic Combustion Laboratory at

Received 29 November 1997; revision received 20 August 2000; accepted for publication 7 February 2001.

*Postdoctoral Researcher, Propulsion Engineering Research Center and Department of Mechanical Engineering; currently Research Scientist, Sandia National Laboratories, MS 9051, P.O. Box 969, Livermore, CA 94551-0969. Member AIAA.

†Senior Research Associate, Propulsion Engineering Research Center and Department of Mechanical Engineering. Member AIAA.

‡Professor, Propulsion Engineering Research Center and Department of Mechanical Engineering. Senior Member AIAA.

Table 1 Rocket test firing conditions

Case	LOX flowrate, kg/s (lb_m/s)	GH_2 flowrate, kg/s (lb_m/s)	$(O/F)_{mass}$	LOX velocity, m/s (ft/s)	GH_2 velocity, m/s (ft/s)	$T_{adiabatic}$, K	$P_{chamber}$, MPa (psi)	c^* efficiency
A	0.09 (0.2)	0.09 (0.2)	1	33.5 (110)	398.7 (1308)	1257	2.96 (429)	1.0
B	0.09 (0.2)	0.05 (0.1)	2	33.5 (110)	199.3 (654)	2033	2.70 (392)	0.96
C	0.09 (0.2)	0.03 (0.067)	3	33.5 (110)	133.5 (438)	2628	2.74 (398)	0.86
D	0.09 (0.2)	0.02 (0.05)	4	33.5 (110)	99.7 (327)	3053	2.84 (412)	0.80

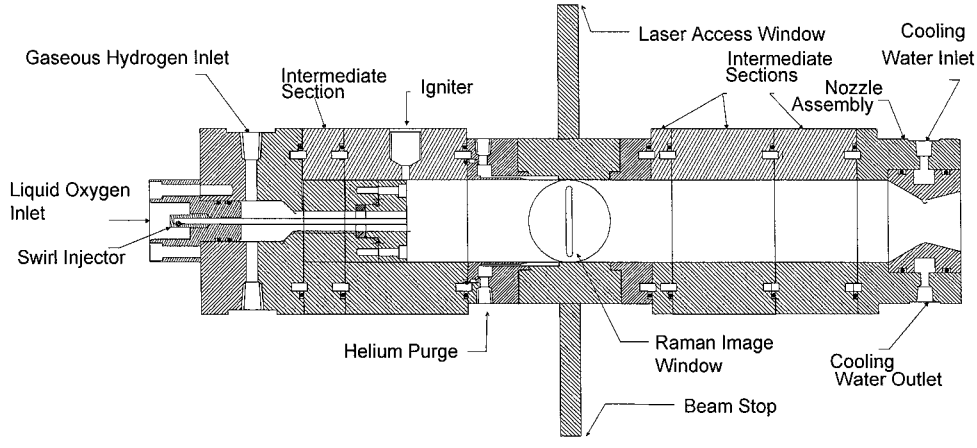

Fig. 1 Cross-sectional view of optically accessible rocket.

Pennsylvania State University. The facility has propellant capabilities for experimental scale combustors. The propellant capabilities include gaseous oxygen (0.5 kg/s), liquid oxygen (0.5 kg/s), gaseous hydrogen (0.1 kg/s), liquid hydrocarbons such as methanol and RP-1 (0.2 kg/s), and air (2.3 kg/s).

An optically accessible, modular rocket chamber is used to study high-temperature, high-pressure combustion. A cross-sectional view of the rocket is displayed in Fig. 1. The internal cross section of the chamber is 50.8×50.8 mm square with 6.35-mm rounded corners. The rocket chamber consists of an injector assembly section, window section, an ignitor section, several blank sections, a transition section from square to round, and a nozzle section that are held together by a hydraulic jack. A major advantage of the design is that it allows optical access for laser-based diagnostics and visualization. The modular nature of the design also allows the placement of the window section along the length of the rocket, thus enabling the study of the combusting flow throughout the chamber length. The length of the rocket can be varied by adding or removing blank sections. For the current work, the length of the chamber from the injector face to the beginning of the nozzle contraction was 311.15 mm. The contraction ratio for the Table 1, case A experiments was 0.0568.

A special optically accessible window section was designed for the Raman spectroscopy experiments. This window section allows a laser beam to penetrate the rocket engine at 90 deg to the general flow direction and pierce through the center of the combustion flowfield. Because the technique is applied in a line measurement configuration, the introduction of the laser beam into the chamber requires only a small access port. However, because the high-energy beam is tightly focused to achieve high spatial resolution in the chamber, a quartz window placed near the vicinity of the focal point is immediately damaged. To circumvent this problem, a small quartz window (12.70 mm in diameter and 6.35 mm thick) was attached at the end of a 12.7-mm (o.d.) stainless steel tube that extended roughly 280 mm from the side wall of the chamber to introduce the laser radiation to the control volume. There was no need to use a window on the downstream side of the control volume. Thus, the laser beam simply exited from the control volume and was blocked by a beam stop that is placed at the end of a stainless steel tube similar to the laser access port. With this configuration, the laser beam cross section at the quartz window location was increased, resulting in lower energy per unit area, without compromising the optical setup. For the present arrangement, the Raman signal is collected 90 deg from the incident laser beam. Consequently, a slotted optical access port on the top of the window section was utilized for signal collection. All of the windows were protected from the extreme temperatures by a small amount of purge gas of helium. Helium does not generate vibrational Raman signatures and, hence, does not directly effect the spectra obtained.

As mentioned earlier, a swirl-coaxial injector element was utilized for introducing the LOX/GH_2 propellants into the chamber. The schematic of the injector can also be seen in Fig. 1. The injector was designed for a nominal LOX flowrate of 0.11 kg/s. The swirl nut seen in the left portion of Fig. 1 is used for imparting swirl to the liquid. The inner and outer diameters of the post measure 3.43 mm and 4.19 mm, respectively. Cold-flow measurements have shown that the swirl angle is 42 deg. Additional details of the swirl post design can be found in Ref. 18. For the fuel-rich experiments described here, an outer diameter of 12.7 mm was chosen for the hydrogen annulus.

Experimental Conditions

Initial studies involving the injector element were conducted for a fixed LOX flow rate of 0.09 kg/s over mixture ratios ranging from one to four. The goal of this phase of experimentation was to document the performance characteristics of the injector element. Detailed flow conditions for four mixture ratios are shown in Table 1. The results show that the c^* efficiency for these experiments decreases with increasing mixture ratio. It is our belief that, for the fixed-injector-geometry case studied here, the lower performance is directly a consequence of poor atomization at the lower fuel/oxidizer momentum ratio. Performance at the higher mixture ratio would have increased if the hydrogen stream momentum were increased by decreasing the cross-sectional area of the fuel annulus.

Raman spectroscopy was set up for making species and temperature measurements at an axial location of 127 mm from the injector face. This axial location corresponds to a length-to-diameter ratio of 37 based on the LOX post diameter of 3.56 mm and was chosen because it represented a sufficient length from the injector face for

substantial vaporization of the LOX. Raman spectroscopy is only suited to liquid free-flow regions because the orders of magnitude more intense Mie scattering from LOX drops overwhelms the inherently weak Raman signal. Initial Raman measurements at this location indicated that only the mixture ratio case of one (case A, Table 1) exhibited a totally LOX-free flowfield. Based on these investigatory experimental results, the technique was applied only for case A (see Table 1) for detailed flowfield measurements at the 127-mm axial measurement location.

Raman Diagnostics Setup

Temperature and major species profiles corresponding to the case A were obtained by linewise spontaneous vibrational–rotational Raman imaging. All of the measurements were done during the steady-state part of the rocket firing. A sample chamber pressure trace for case A indicating the Raman data collection timing is shown in Fig. 2.

Single-shot Raman images were gathered while the chamber pressure was steady, which took place approximately 8 s after ignition of the flow. This delay is associated with achieving good quality LOX conditions at the injector. A pulse laser operation frequency of 5 Hz was chosen to allow enough time for data transfer to occur.

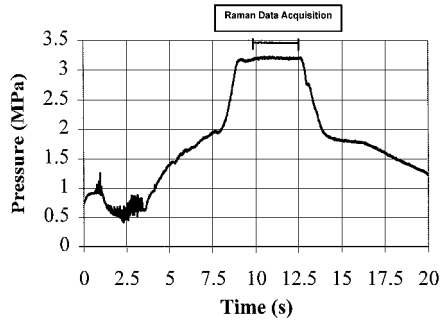

Fig. 2 Sample pressure trace from typical rocket test case.

This 5-Hz frequency enabled roughly 15 single-shot Raman images to be captured during each rocket firing.

A schematic of the Raman system is shown in Fig. 3. A Q-switched, frequency-doubled Nd:YAG laser operating at 5 Hz was used as the 532-nm excitation source. The laser power output was measured to be about 300 mJ/pulse and the pulse duration was determined to be 5 ns. The laser pulse polarization was rotated from the vertical to horizontal direction via two mirrors immediately following the laser. This allowed the collection optics to be in the correct polarization orientation. The laser beam was passed through the window section that separates the test cell from the instrument cell and reflected by two mirrors to position it in line with the rocket window section. The laser beam was then focused to a 500 μm diameter at the center of the rocket cross section by an $f = 0.75$ m focusing lens. A linewise Raman image of the flame front was projected by a 76.2-mm-diam mirror placed above the rocket window section. The image was gathered and focused by an $f/\#$ 1.8, 105-mm Nikon lens. An $f/\#$ 1.8 Kaiser Optic holographic imaging spectrograph, in conjunction with an intensified charge-coupled device (ICCD) (576 × 384 pixel) camera, was used to capture the Raman signals of major combustion species (H_2, O_2, H_2O). The gate width of the ICCD was 5 ns, and it corresponded to the exact timing of the laser beam passage through the rocket engine. The system allowed simultaneous multispecies multipoint Raman measurements. The slit width of 500 μm and binning of 4 pixels in the radial dimension, corresponding to the 384-pixel direction, and of 6 pixels in the wavelength dimension, corresponding to the 576-pixel direction, were used. The Raman signal-to-noise ratio was increased by discriminating against the Rayleigh interference by the use of a notch filter centered at 532 nm, that has full width at half maximum (FWHM) of 18 nm, (FWHM ≈ 18 nm) placed inside the spectrograph. The intense flame interference was reduced 50% by the use of a linear dichroic sheet polarizer aligned with the Raman signal polarization. Further discrimination against the flame luminosity was achieved by the use of a sharp infrared (IR) filter. The background radiation for these high-temperature, high-pressure LOX/GH_2 flames has been studied and determined to be a continuous source between IR and UV.[17] The same study also revealed that the flame luminosity is a weak function of mixture

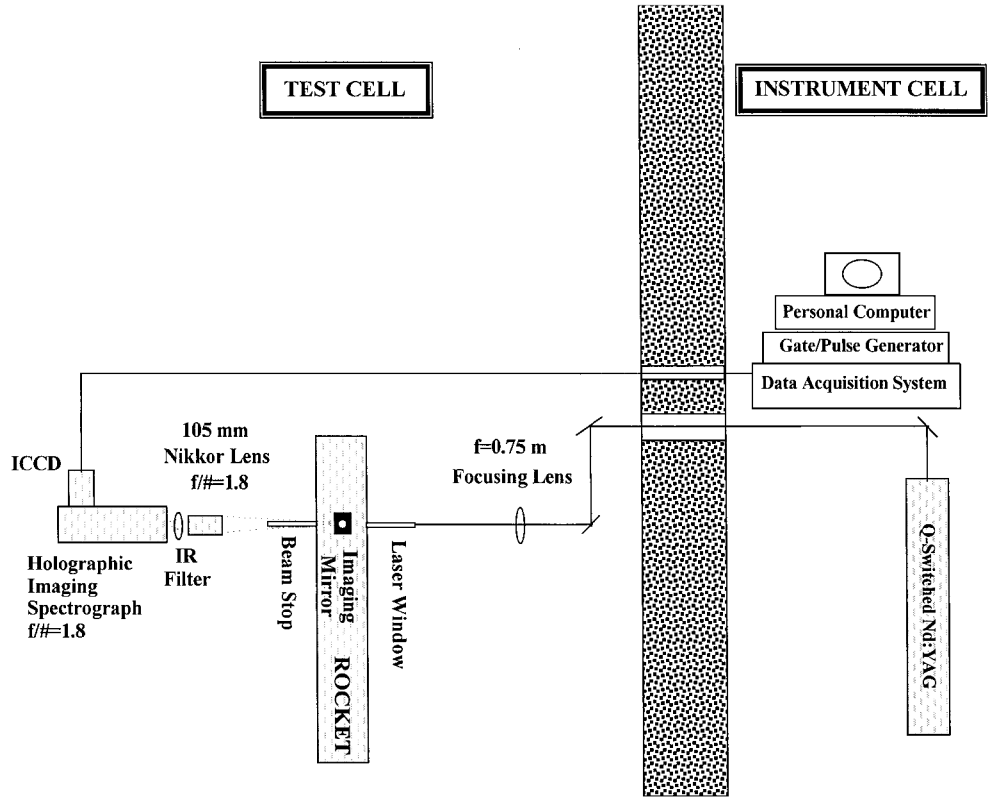

Fig. 3 Schematic of Raman setup.

ratio (O/F) but a strong function of chamber pressure. The current diagnostics system allowed enough Raman signal under the studied flame conditions to obtain single-shot Raman data. A similar diagnostics system may be rendered useless for single-shot data if it is used with different combustion conditions, namely higher pressures and temperatures, due to higher background radiation.

Results and Discussion

The major species mole fractions and temperature can be obtained from the wavelength averaged vibrational Raman signal intensity values. Raman signal intensity of a given species i is related to the number density of the molecule, a constant, and a temperature-dependent function that relates the spectral bandwidth factor to the Raman signal strength as represented by Eq. (1):

$$S_i = n_i K_i f_i(T) \tag{1}$$

The constant in this equation accounts for the laser pulse energy, species Raman cross section, optical collection efficiency, and optical solid angle.

Once the Raman signals from the different species are collected by the ICCD camera, they are converted into mole fraction and temperature profiles across the measured rocket combustion chamber with calibration curve fit values and an assumption of ideal gas law behavior.

The signal intensity for a typical instantaneous unprocessed image for a rocket firing corresponding to case A (see Table 1) is plotted as a three-dimensional graph in Fig. 4. In Fig. 4, the Raman signal intensity is plotted vs the wavelength and radial location dimensions. As seen in Fig. 4, Raman Stokes rotational hydrogen lines are also measured because of the relatively larger Raman cross section of hydrogen. The holographic grating reciprocal linear dispersion of 11.1 nm/mm allows the hydrogen vibrational Stokes lines and the rotational Stokes lines to be captured simultaneously on the camera. The efficiency of the grating combined with the efficiency of the camera at these wavelength regions introduce higher signal counts for the rotational hydrogen lines as compared to theoretical values. Theoretically, the S-branch rotational hydrogen Raman signal intensity should be about half of the magnitude observed for the vibrational Raman signal intensity at 1200 K for a camera with uniform response for the entire wavelength domain. The Raman signal from water vapor is also seen in Fig. 4. However, a close inspection of this Fig. 4 revealed the total absence of an oxygen Raman signal that would occur at around 580 nm. Hydrogen rotational lines generate the only signal found at this spectral location. This indicates that, at this axial location, all of the oxygen is consumed.

To obtain the flowfield species mole fraction and temperature, the optical setup was first calibrated using a laminar hydrogen/air flame from a flashback-resistant, flat flame, Krupa et al. style burner.[21] Mole fractions of hydrogen and air were varied to obtain various equivalence ratios. The temperature at these different flame conditions were measured with an uncoated B-type (platinum–30% rhodium vs platinum–6% rhodium) thermocouple with a bead diameter of ~385 μm. The calibration results are displayed in Figs. 5 and 6. The accuracy of the temperature and mole fraction measurements could be improved further by increasing the number of Raman signal accumulations during calibration data acquisition. More details about the uncertainty in single-shot measurements are included in the following section.

From the calibration procedure, $f(T)$ and K for each major species are generated. The assumption of the ideal gas law allows an iterative data reduction process once the Raman signal for each species across the rocket engine combustion zone is obtained. The process assumes a temperature value and calculates the total number density per mole at a given location. If the number of molecules per mole equals Avogadro's number, then the temperature and mole fraction of each species are accepted, otherwise a new temperature value is assumed. With this data reduction procedure, single-shot temperature and mole fraction profiles of LOX/GH_2 combustion at

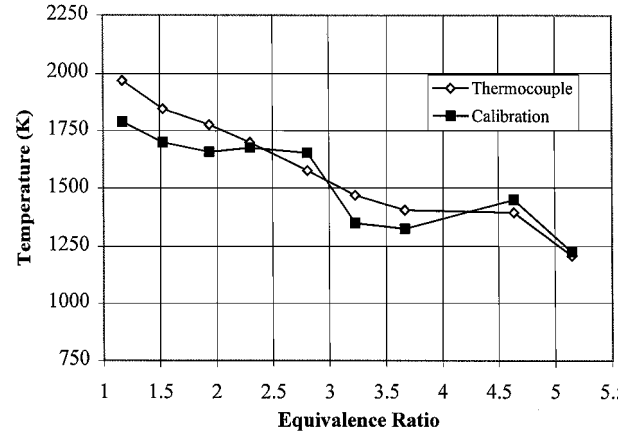

Fig. 5 Calibration temperature comparison.

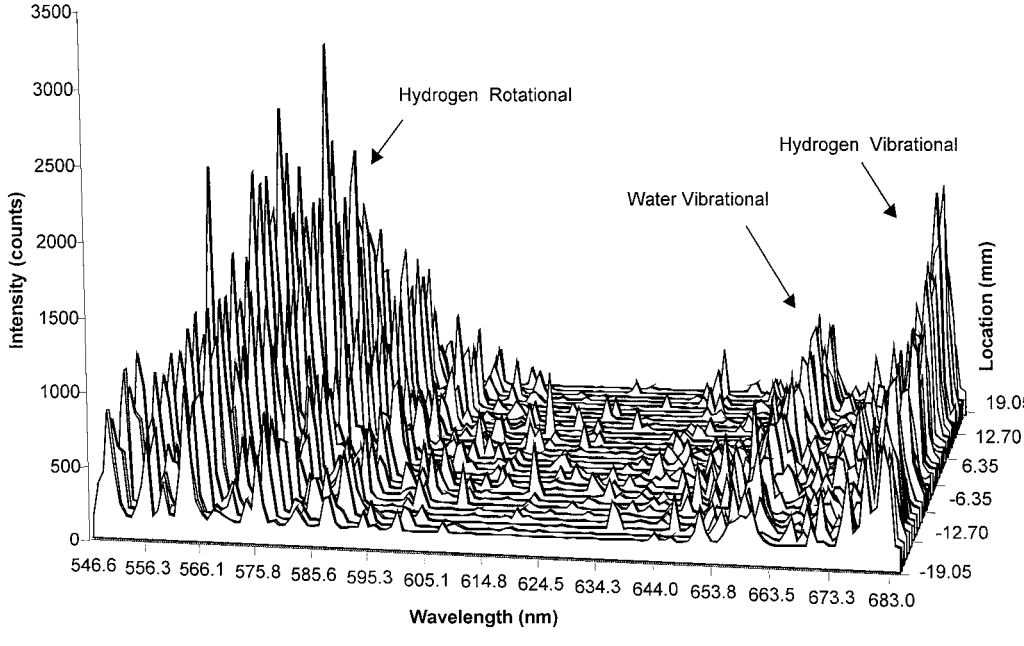

Fig. 4 Typical instantaneous unprocessed Raman image; axial measurement location is 127 mm from injector face.

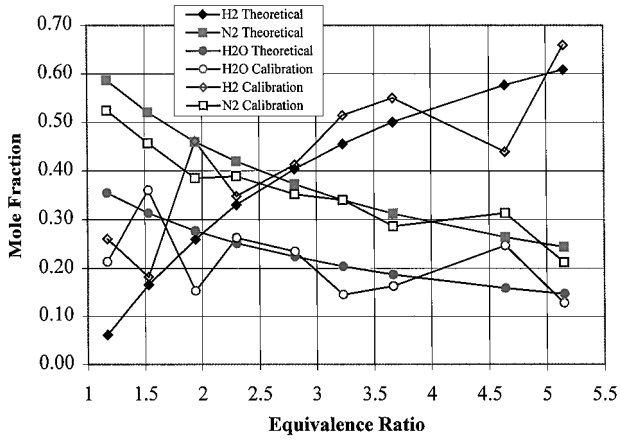

Fig. 6 Calibration species mole fraction comparison.

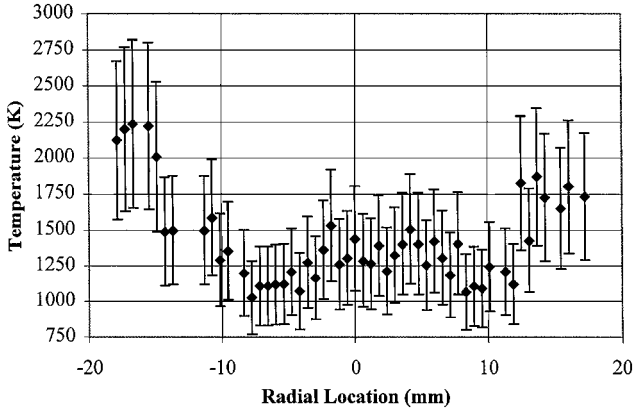

Fig. 7 Single-shot temperature profile.

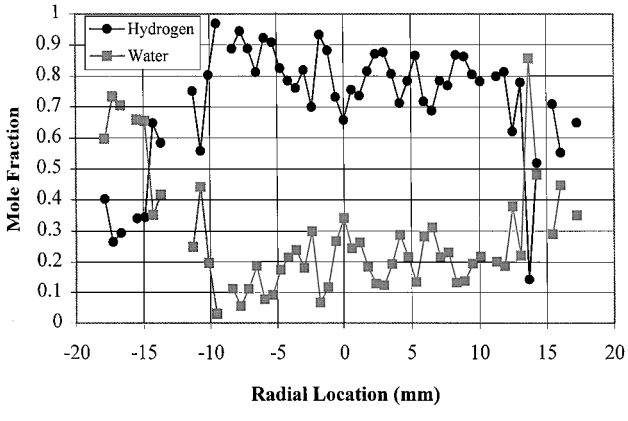

Fig. 8 Single-shot species mole fraction profile.

the mixture fraction of one (case A, Table1) were obtained for the 127-mm axial measurement location. To the authors' knowledge, these measurements represent the first attempt at single-shot temperature and major species mole fraction profile measurements of LOX/GH_2 propellant combustion in a rocket engine under relatively high pressure and temperature conditions. Sample instantaneous radial profiles of temperature and species mole fractions are shown in Figs. 7 and 8.

Note that the adiabatic flame temperature predictions of 1250 K is close to the temperature measurements at the center region of the chamber. The temperature profiles indicate increased values close to the wall region of the chamber as compared to the central region. The measurements indicate larger noise at the edges of the Raman images (near the walls), which contribute to the uncertainty in the temperature values. This noise is believed to arrive from the intense laser beam reflection from the laser window and the beam dump.

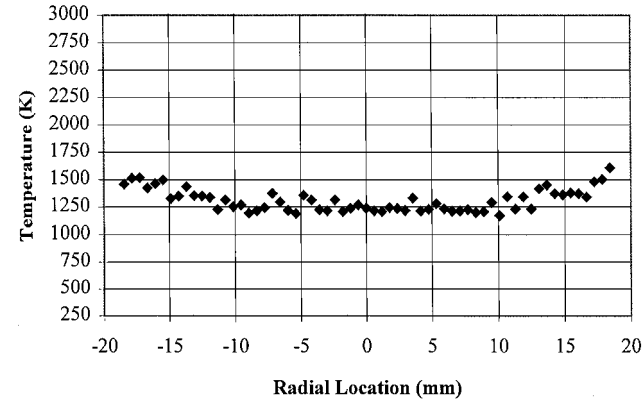

Fig. 9 Rocket engine temperature profile from average of 26 single-shot Raman images.

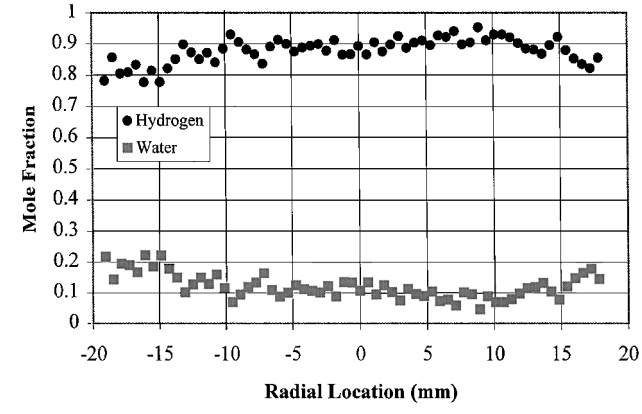

Fig. 10 Rocket engine major species profiles from average of 26 single-shot Raman images.

After the single-shot temperature and mole fraction profiles were obtained, the temporally averaged results were obtained. Figures 9 and 10 display the resultant average temperature and mole fraction profiles from 26 single-shot Raman images.

The average temperature profile is much more uniform and is close to the adiabatic temperature value of 1250 K. However, there is still a slight increase in the temperature at the wall regions of the rocket chamber compared to the central region. This may be due to mixing nonuniformity. One possible explanation is that there is a higher oxygen concentration near the walls creating a more oxygen-rich, closer to stoichiometric environment leading to higher temperature values. Another explanation for the temperature rise near the wall may be that the averaging effect is stronger in the central regions of the flow than the near wall regions, hence, the lower temperature values at the central region.

Error Analysis

The error bars associated with the single-shot temperature values are derived from Eq. (2) (Ref. 22):

$$\delta R = \left\{ \sum_{i=1}^{N} \left(\frac{\partial R}{\partial X_i} \delta X_i \right)^2 \right\}^{\frac{1}{2}} \tag{2}$$

where R is replaced by number density n_i and X_i is replaced by the independent variables of Eq. (1), namely, Raman signal intensity S_i, constant K_i, and temperature-dependent function $f_i(T)$. By the incorporation of the constant K_i into the equation $f_i(T)$, the following equation is obtained:

$$\delta n_i = \left\{ \left(\frac{\partial n_i}{\partial N_i} \delta N_i \right)^2 + \left(\frac{\partial n_i}{\partial f_i(T)} \delta f_i(T) \right)^2 \right\}^{\frac{1}{2}} \tag{3}$$

After performing the partial derivatives in Eq. (3), the statistical uncertainty equation takes on the form of Eq. (4):

$$\delta n_i = \left\{ [f_i(T)\delta N_i]^2 + [N_i \delta f_i(T)]^2 \right\}^{\frac{1}{2}} \tag{4}$$

The first term of Eq. (4) reflects the errors due to uncertainty in measuring Raman signal intensity. This uncertainty value is developed by the following equation:

$$\delta N_i = \left\{ \left(\sigma_{S_i}\right)^2 + \left(\sigma_{B_i}\right)^2 + (\sigma_R)^2 + (\sigma_D)^2 \right\}^{\frac{1}{2}} \tag{5}$$

where σ_S and σ_B refer to signal and flame luminosity interference shot noise and σ_R and σ_D refer to readout noise and dark current noise, respectively. Readout noise (~1 counts) and dark current noise of the intensifier (~5 counts) and the ICCD (~2 counts) are negligible compared to the signal and flame luminosity shot noise (~50 counts). Combination of about 10% quantum efficiency and the high gain of the intensifier results in signal and background interference shot noise that dominates the uncertainty in the error estimate of the measurements.

The second term of Eq. (4) reflects the error due to calibration uncertainty. The standard deviation of the calibration measurements reveal an average of 18% uncertainty in calibration of H_2O number density and 20% uncertainty in calibration of H_2 number density. It is assumed that the overall error in calibration is equal to the average of the individual uncertainty values, that is, ~19%.

The uncertainty in measuring number density of the major LOX/GH_2 combustion species results in the uncertainty of temperature and species mole fraction values. Single-shot temperature-profile error bars include both the measurement uncertainty and the calibration uncertainty. The measurement uncertainty is due to inherently noisy operation of the ICCD, whereas the uncertainty related to the calibration is due to the low signal-to-noise ratio of the calibration Raman measurements. These low signal-to-noise value calibration Raman measurements can be improved roughly 2.5 times by increasing the number of accumulations from 15 to 100.

In summary, the standard deviation based on number density indicates that the signal detection uncertainty of about 10% and calibration uncertainty of about 19% contributes to the measurements. This uncertainty in number density is reflected in the single-shot temperature values of Fig. 7. In terms of temperature values, uncertainty in calibration constitutes roughly 75% and uncertainty in signal and background flame luminosity shot noise constitutes the remaining 25% of the error bars. However, the uncertainty due to calibration can be reduced by a factor of 2.5 by increasing the number of accumulations from 15 to 100 shots.

Conclusions

Multispecies, linewise Raman imaging of LOX/GH_2 combustion at high pressure and temperature was conducted at oxidizer-to-fuel mass ratio, $(O/F)_{mass}$, of unity. Single-shot temperature and major species profiles were measured. The profiles indicate relatively high temperature values at the wall regions of the rocket chamber and close to adiabatic flame temperatures at the center region of the chamber. With 26 single-shot images, averaged temperature and concentration profiles were obtained. A similar trend of higher temperature values close to the walls of the rocket chamber and adiabatic flame temperature values at the central location of the rocket was also observed for the averaged Raman data. Error analysis of the data revealed that improvements to the single-shot data accuracy (~19%) are possible with a higher number of accumulations during the calibration data acquisition procedure. The higher than adiabatic flame temperature values indicate the need for further investigation of such flames.

Acknowledgments

The authors acknowledge funding from NASA Marshall Space Flight Center Cooperative Agreement Grant NCC 8-46. The authors thank L. Schaaf for his help in conducting the experiments.

References

[1]Eckbreth, A. C., "Laser Diagnostics for Combustion Temperature and Species," *Energy and Engineering Sciences Series*, 1st ed., Vol. 7, Abacus, Cambridge, MA, 1988.

[2]Barlow, R. S., Carter, C. D., "Raman/Rayleigh/LIF Measurements of Nitric Oxide Formation in Turbulent Hydrogen Jet Flames," *Combustion and Flame*, Vol. 97, No. 3–4, 1994, pp. 261–280.

[3]Cheng, T. S., Wehrmeyer, J. A., and Pitz, R. W., "Simultaneous Temperature and Multispecies Measurements in Lifted Hydrogen Diffusion Flame," *Journal of Combustion and Flame*, Vol. 91, No. 3–4, 1992, pp. 323–345.

[4]Drake, M. C., Lapp, M., and Penney, C. M., "Use of Vibrational Raman Effect for Gas Temperature Measurements," *Temperature: Its Measurements and Control in Science and Industry*, Vol. 5, 1982, pp. 631–638.

[5]Eckbreth, A. C., Bonczyk, P. A., and Verdieck, J. F., "Combustion Diagnostics by Laser Raman and Fluorescence Techniques," *Progress in Energy and Combustion Science*, Vol. 5, No. 4, 1979, pp. 253–323.

[6]Lapp, M., Penney, C. M., and Asher, J. A., "Application of Light Scattering Techniques for Measurements of Density, Temperature and Velocity in Gas Dynamics," National Technical Information Service AD-759575, 1973.

[7]Lederman, S., "The Use of Laser Raman Diagnostics in Flow Field and Combustion," *Progress in Energy and Combustion Science*, Vol. 3, No. 1, 1977, pp.1–33.

[8]Yaney, P. P., Becker, R. J., Magill, P. D., and Danset, P., "Dynamic Temperature Measurements of Flames Using Spontaneous Raman Scattering," *Temperature: Its Measurements and Control in Science and Industry*, Vol. 5, 1982, pp. 639–648.

[9]Foust, M. J., Deshpande, M., Pal, S., Ni, T., Merkle, C. L., and Santoro, R. J., "Experimental and Analytical Characterization of Shear Coaxial Combusting GO_2/GH_2 Flowfield," AIAA Paper 96-0646, Jan. 1996.

[10]Foust, M. J., Pal, S., and Santoro, R. J., "Gaseous Propellant Rocket Studies Using Raman Spectroscopy," AIAA Paper 96-2766, July 1996.

[11]Farhangi, S., Gylys, V. T., and Jensen, R. J., "Gas Composition and Temperature Measurements in a Rocket Engine Combustor Using Raman Technique," AIAA Paper 94-0225, Jan. 1994.

[12]DeGroot, W. A., "Species and Temperature in H_2/O_2 Rocket Flowfields by Means of Raman Scattering Diagnostics," AIAA Paper 92-3353, July 1992.

[13]Williams, D. R., Mckeown, D., Porte, F. M., Baker, C. A., Astill, A. G., and Rawley, K. M., "Coherent Anti-Stokes Raman Spectroscopy (CARS) and Laser-Induced Fluorescence (LIF) Measurements in a Rocket Engine Plume," *Combustion and Flame*, Vol. 94, No. 1–2, 1994, pp. 77–90.

[14]Moser, M. D., Merenich, J. J., Pal, S., Santoro, R. J., "OH-Radical Imaging and Velocity Field Measurements in a Gaseous Hydrogen/Oxygen Rocket," AIAA Paper 93-2036, June 1993.

[15]Pal, S., Moser, M. D., Ryan, H. M., Foust, M. J., and Santoro, R. J., "Shear Coaxial Injector Atomization Phenomena for Combusting and Non-Combusting Conditions," *Journal of Atomization and Sprays*, Vol. 6, No. 2, 1996, pp. 227–244.

[16]Mayer, W., and Tamura, H., "Flow Visualization of Supercritical Propellant Injection in a Firing LOX/GH_2 Rocket Engine," AIAA Paper 95-2433, July 1995.

[17]Mayer, W., Schik, A., Schweitzer, C., and Schaffler, M., "Injection and Mixing Processes in High Pressure LOX/GH_2 Rocket Combustors," AIAA Paper 96-2620, July 1996.

[18]Rahman, S. A., Pal, S., and Santoro, R. J., "Swirl Coaxial Atomization; Cold Flow and Hot-Fire Experiments," AIAA Paper 95-0381, Jan. 1995.

[19]Beisler, M. A., Pal, S., Moser, M. D., and Santoro, R. J., "Shear Coaxial Injector Atomization in a LOX/GH_2 Propellant Rocket," AIAA Paper 94-2775, June 1994.

[20]Wehrmeyer, J. A., Cramer, J. M., Eskridge, R. H., and Dobson, C. C., "Ultraviolet Raman Diagnostics for Rocket Engine Injector Development," AIAA Paper 97-2843, July 1997.

[21]Krupa, R. J., Culberth, T. F., Smith, B. W., and Winefordner, J. D., "A Flashback-Resistant Burner for Combustion Diagnostics and Analytical Spectrometry," *Journal of Applied Spectroscopy*, Vol. 40, No. 6, 1986, pp. 729–733.

[22]Moffat, R. J., "Describing the Uncertainties in Experimental Results," *Experimental and Thermal Fluid Science Journal*, Vol. 1, No. 1, 1988, pp. 3–17.